Electromagnetic-Wave Propagation in a Conducting Waveguide Loaded with a Tape Helix

HAN S. UHM AND JOON Y. CHOE

Abstract—**Dispersion properties of the electromagnetic (EM) waves, propagating through a tape helix located inside a waveguide, are investigated. A complete dispersion relation for the eigenfrequency ω and the axial wavenumber k is obtained, including influence of the outer conducting wall on the EM-wave propagation. It is shown that the limiting case where the outer conducting wall is very close to the helix, the helix mode is nearly a straight line in the (ω, k) parameter space, and is independent of the width of the helix tape. Moreover, contrary to the conventional helix theory, the outer conducting wall completely eliminates the forbidden regions in the (ω, k) parameter space.**

I. INTRODUCTION

ONE OF THE slow-wave structures that has been used frequently in a wide-band microwave amplification is the helix waveguide [1]–[10]. Except for a limited study [10] of the fast waves in a dielectric-loaded helix waveguide, previous analyses of dispersion properties in a helix waveguide have been *mostly* restricted to the helix itself, without proper investigation of the important influence of an outer conducting wall on behavior of the electromagnetic (EM) wave propagation. Particularly, previous papers [1]–[9] have been concentrated on the slow-wave dispersion properties, where the phase velocity of the EM wave is less than the speed of light *in vacuo*. Although this limited analysis is reasonable in the application on the traveling-wave tube where the electron-beam mode is less than the speed of light, for newly developed microwave devices such as the gyrotrons [11]–[14], the magnetrons [15], and the free-electron laser [16], [17], we are urged to improve the theory of the helix waveguide modes, including the fast wave. These new microwave tubes frequently utilize coupling of the electron-beam mode with the fast wave.

This paper develops a theory of the dispersion properties of the EM-wave propagation in a tape-helix-loaded waveguide. The present work extends the previous theory [18] developed by the authors for an idealized sheath helix, to a more realistic tape helix. Dispersion relation of a tape helix without an outer conducting wall has been presented in various previous papers [3], [4]. However, because of lack of the fast-wave portion in the dispersion relation, previous results exhibit periodic appearance of the forbidden regions in the (ω, k) parameter space, where ω and k are the eigenfrequency and the axial wavenumber, respectively. The fast-wave portion of the EM dispersion relation shows up only for an inclusion of the outer conducting wall or for an inclusion of a dielectric material [10]. In this regard, in Section II, we obtain the full dispersion relation ((24) and (25)) of the electromagnetic waves in a helix-loaded waveguide, including the important influence of the outer conducting wall.

In the limiting case when the outer conducting wall approaches close to the helix, it is shown that the dispersion relation is reduced to three simple distinctive relations. These are the transverse electric-like (TE-like), the transverse magnetic-like (TM-like), and the helix modes. Remarkably, the helix mode in this limit is identical to the result [18] obtained for an idealized sheath helix, thereby *not* depending on a moderate value of helix tape width. Moreover, presence of the outer conducting wall completely eliminates the forbidden regions in the (ω, k) parameter space. On the other hand, when the outer conducting wall is removed from the helix to infinity, the present dispersion relation recovers the previous result obtained by Sensiper [4]. In Section III, the full dispersion relation is numerically investigated for a broad range of system parameters. It is shown from the numerical analysis that the dispersion curves of the helix mode wiggle more strikingly as the outer conducting wall is further removed from the helix to infinity. In addition, we find that there are infinite numbers of hybrid waves which consist mostly of combinations of the TE- and TM-like modes.

In a broad sense, the full dispersion relation in (24) and (25) of the electromagnetic waves in a helix-loaded waveguide also includes the transmission line physics where the plane waves and lump circuit analysis prevail. Moreover, the transmission line physics emphasizes the surface wave locally concentrated on the surface of the tape helix, thereby allowing propagation of near-zero frequency. Obviously from Section III, the dispersion relation in (24) and (25) describes both the slow waves corresponding to the transmission line and the fast hybrid waves, which explicitly exhibit the cutoff frequency. The forbidden region in the (ω, k) parameter space is important in the antenna theory, because of radial radiation of the EM-wave energy. However, enclosure of the helix circuit with a conducting wall

Manuscript received July 7, 1982; revised May 2, 1983. This work was supported by the Independent Research Fund at the Naval Surface Weapons Center.

The authors are with the Naval Surface Weapons Center, White Oak, Silver Spring, MD 20910.

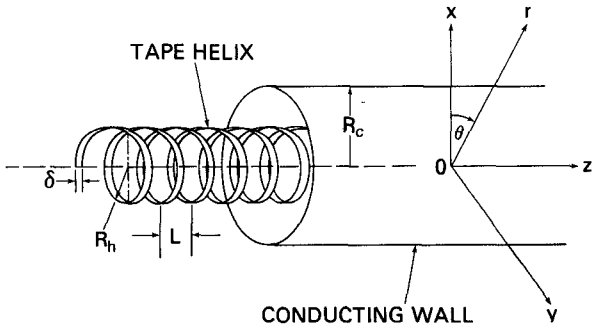

Fig. 1. System configuration and cylindrical coordinates.

withholds radial dissipation of the EM-wave energy, thereby prohibiting the radiation. From a mathematical point of view, the radial profile of the EM waves in the forbidden region is described by a modified Bessel function, which decreases monotonically along the radial direction. On the other hand, in the presence of the outer conducting wall, the radial profile of the wave is described by an ordinary Bessel function, clearly indicating a pattern of a standing wave in the radial direction. In this regard, presence of the outer conducting wall completely eliminates the forbidden region, allowing the propagation of the EM waves along the axial direction.

II. Dispersion Relation for Tape Helix

A realistic representative physical model of the wire helix is the tape helix shown in Fig. 1, where a helix tape with width δ and zero thickness is located inside a conducting waveguide with radius R_c. The radius and pitch of the helix are denoted by R_h and L, respectively. We, therefore, define the pitch angle ϕ by

$$\cot\phi = 2\pi R_h/L. \tag{1}$$

As illustrated in Fig. 1, cylindrical polar coordinates (r, θ, z) are introduced in the present analysis.

Application of Floquet's theorem shows that when the helix is moved a distance L in the z-direction, it coincides with itself. Thus the z-dependence of the fields must be of the form

$$\exp(ik_m z) = \exp\{i(k - 2\pi m/L)z\}$$

where m is an integer (i.e., $m = 0, \pm 1, \pm 2, \cdots$) and k is the axial wavenumber. It is also seen that if the helix is moved a distance less than L and then rotated in θ through a certain angle, it again coincides with itself. Consider the general form of the EM field $\psi(x, t)$ having the foregoing z-dependence

$$\psi(x,t) = \sum_{n,m} \hat{\psi}_{n,m}(r)\exp\left\{i\left[n\theta + \left(k - m\frac{2\pi}{L}\right)z - \omega t\right]\right\} \tag{2}$$

where the azimuthal harmonic number n is also an integer $(n = 0, \pm 1, \pm 2, \cdots)$ and ω is the eigenfrequency. Replacing z and θ in (2) by $z' + z$ and $\theta' + 2\pi z/L$, respectively, we obtain

$$\psi(x',t) = \exp\{i(kz - \omega t)\}\sum_{n,m}\hat{\psi}_{n,m}(r) \cdot\exp\left\{i\left[n\theta' + \left(k - m\frac{2\pi}{L}\right)z' + (n-m)\frac{2\pi}{L}z\right]\right\}. \tag{3}$$

According to Floquet's theorem, the solution as a function of θ' and z' must be of the same form as it is as a function of θ and z. To ensure this, it is necessary to take [3]

$$m = n - l \tag{4}$$

and for $m \neq n - l$ to put $\psi_{n,m} = 0$. In (4) the space harmonic number $l = n - m$ is an arbitrary integer. In this regard, all components of the EM field are assumed to vary according to

$$\psi(x,t) = \sum_{n=-\infty}^{\infty}\hat{\psi}_n(r)\exp\{i(n\theta + k_n z - \omega t)\}. \tag{5}$$

where the total axial wavenumber k_n is defined by

$$k_n = k - (n-l)\frac{2\pi}{L}. \tag{6}$$

The Maxwell equations for the electric and magnetic field amplitudes can be expressed as

$$\begin{aligned}\nabla\times\hat{\boldsymbol{E}}(x) &= i(\omega/c)\hat{\boldsymbol{B}}(x)\\ \nabla\times\hat{\boldsymbol{B}}(x) &= (4\pi/c)\hat{\boldsymbol{J}}(x) - i(\omega/c)\hat{\boldsymbol{E}}(x)\end{aligned} \tag{7}$$

where c is the speed of light *in vacuo*, $\hat{\boldsymbol{E}}(x)$ and $\hat{\boldsymbol{B}}(x)$ are the electric and magnetic fields, and the electric current density $\hat{\boldsymbol{J}}(x)$ vanishes except at $r = R_h$. Making use of (7), for the azimuthal mode number n, it is straightforward to show that the differential equation for the axial components of the electric and magnetic fields is given by

$$\left(\frac{1}{r}\frac{\partial}{\partial r}r\frac{\partial}{\partial r} - \frac{n^2}{r^2} + \frac{\omega^2}{c^2} - k_n^2\right)\begin{Bmatrix}\hat{E}_{zn}\ (r)\\ \hat{B}_{zn}\ (r)\end{Bmatrix} = 0 \tag{8}$$

except at $r = R_h$. Therefore, the physically acceptable solution to (8) is

$$\hat{E}_z(x) = \sum_n a_n\exp\{i(n\theta + k_n z)\} \times\begin{cases} J_n(p_n r), & 0 \leqslant r \leqslant R_h\\ J_n(\eta_n)\dfrac{N_n(\zeta_n)J_n(p_n r) - J_n(\zeta_n)N_n(p_n r)}{J_n(\eta_n)N_n(\zeta_n) - J_n(\zeta_n)N_n(\eta_n)}, & R_h \leqslant r \leqslant R_c\end{cases} \tag{9}$$

for the electric field and

$$\hat{B}_z(x) = \sum_n b_n\exp\{i(n\theta + k_n z)\} \times\begin{cases} J_n(p_n r), & 0 \leqslant r < R_h\\ J_n'(\eta_n)\dfrac{N_n'(\zeta_n)J_n(p_n r) - J_n'(\zeta_n)N_n(p_n r)}{J_n'(\eta_n)N_n'(\zeta_n) - J_n'(\zeta_n)N_n'(\eta_n)}, & R_h < r \leqslant R_c\end{cases} \tag{10}$$

for the magnetic field. In (9) and (10), a_n and b_n are constants, $J_n(x)$ and $N_n(x)$ are the Bessel functions of the first and second kinds, respectively, of order n, the prime ($'$) denotes $(d/dx)J_n(x)$ and $(d/dx)N_n(x)$, and the parameters η_n, ζ_n, and p_n are defined by

$$\eta_n^2 = \zeta_n^2 R_h^2/R_c^2 = p_n^2 R_h^2 = \left(\omega^2/c^2 - k_n^2\right)R_h^2. \quad (11)$$

In obtaining (9) and (10), use has been made of the boundary conditions so that the tangential electric field is continuous for all θ and z-directions.

The additional boundary conditions at $r = R_h$ for the tape helix are derived from the property that the discontinuity in tangential magnetic field is equal to the total surface current density. These are

$$\hat{B}_z^i - \hat{B}_z^o = \frac{4\pi}{c}\hat{J}_\parallel \cos\phi \quad (12)$$

and

$$\hat{B}_\theta^o - \hat{B}_\theta^i = \frac{4\pi}{c}\hat{J}_\parallel \sin\phi \quad (13)$$

where the superscripts i and o represent $\hat{\psi}^i = \lim_{\epsilon \to 0_+}\hat{\psi}(R_h - \epsilon, \theta, z)$ and $\hat{\psi}^o = \lim_{\epsilon \to 0_+}\hat{\psi}(R_h + \epsilon, \theta, z)$, respectively, $\hat{J}_\parallel(r = R_h, \theta, z)$ is the surface current density along the helix direction with the unit vector

$$\hat{e}_\phi = \cos\phi\hat{e}_\theta + \sin\phi\hat{e}_z \quad (14)$$

and $\hat{e}_\theta$ and $\hat{e}_z$ are unit vectors in the azimuthal and axial directions.

For regions, small compared to a free-space wavelength, the fields are solutions to Laplace's equation and are like static fields. We, therefore, assume that the current in the tape flows only in the tape direction, that it does not vary in phase or amplitude over the width of the tape, and that its phase variation in the direction of the tape corresponds to $l\theta + kz$ for θ and z corresponding to a point moving along the centerline of the tape [3], [4]. Within the context of these assumptions, the surface current density $\hat{J}_\parallel$ in (13) is expressed as

$$\hat{J}_\parallel = \begin{cases} \hat{J}\exp\{i(l + Lk/2\pi)\theta\}, & L\theta/2\pi < z < L\theta/2\pi + \delta \\ 0, & \text{elsewhere.} \end{cases} \quad (15)$$

Fourier decomposing this current density, we obtain

$$\hat{J}_\parallel = \sum_n j_{\parallel n}\exp\{i(n\theta + k_n z)\} \quad (16)$$

where the component amplitude $j_{\parallel n}$ is defined by

$$j_{\parallel n} = \frac{\delta}{L}\hat{J}\exp(-ik_n\delta/2)\frac{\sin(k_n\delta/2)}{k_n\delta/2}. \quad (17)$$

The constants a_n and b_n in (9) and (10) can be expressed in terms of the component amplitude $j_{\parallel n}$ of the surface current density at helix, by making use of the boundary conditions in (12) and (13). Substituting (10) and (16) into (12), we obtain

$$b_n = \frac{2\pi^2}{c}j_{\parallel n}\cos\phi\,\eta_n\frac{J_n'(\zeta_n)N_n'(\eta_n) - J_n'(\eta_n)N_n'(\zeta_n)}{J_n'(\zeta_n)} \quad (18)$$

where use has been made of the Bessel function identity

$$J_n(x)N_n'(x) - J_n'(x)N_n(x) = 2/\pi x.$$

Similarly, the constant a_n is given by

$$a_n = -i\frac{p_n}{\omega}2\pi^2 j_{\parallel n}\eta_n\cos\phi\left(\tan\phi - \frac{k_n n}{\eta_n p_n}\right) \times \frac{J_n(\zeta_n)N_n(\eta_n) - J_n(\eta_n)N_n(\zeta_n)}{J_n(\zeta_n)}. \quad (19)$$

For further analysis, we assume that at the helix surface, the electric field along the helix direction is set equal to zero along the center line of the tape, i.e.,

$$\hat{E}_\parallel = (\hat{E}\cdot\hat{e}_\theta)_{r=R_h} = 0 \quad (20)$$

at $z = (L\theta/2\pi) + (\delta/2)$. This assumption satisfies the boundary conditions on electric field approximately. However, the approximation is good for narrow tapes [3], [4]. Obviously from (14) and (20) we obtain

$$\hat{E}_\parallel = \hat{E}_\theta(R_h)\cos\phi + \hat{E}_z(R_h)\sin\phi. \quad (21)$$

Making use of the Maxwell equation (7), we can show that the component of the azimuthal mode number n for the electric field $\hat{E}_\parallel$ is expressed as

$$\hat{E}_{\parallel n} = \left\{a_n J_n(\eta_n)\cos\phi\left(\tan\phi - \frac{k_n n}{\eta_n p_n}\right) - i\frac{\omega}{cp_n}\cos\phi\, b_n J_n'(\eta_n)\right\}\exp\{i(n\theta + k_n z)\}. \quad (22)$$

Eliminating the constants a_n ad b_n in favor of $j_{\parallel n}$ gives

$$\hat{E}_\parallel = -i\frac{2\pi^2}{\omega R_h}\cos^2\phi\sum_n \exp\{i(n\theta + k_n z)\}j_{\parallel n} \times \left\{\eta_n^2\left(\tan\phi - \frac{k_n n}{\eta_n p_n}\right)^2\frac{J_n(\eta_n)}{J_n(\zeta_n)} \cdot\left[J_n(\zeta_n)N_n(\eta_n) - J_n(\eta_n)N_n(\zeta_n)\right] + \frac{\omega^2 R_h^2}{c^2}\frac{J_n'(\eta_n)}{J_n'(\zeta_n)} \cdot\left[J_n'(\zeta_n)N_n'(\eta_n) - J_n'(\eta_n)N_n'(\zeta_n)\right]\right\}. \quad (23)$$

This electric field is to be set equal to zero along the center line of the tape, i.e., at $z = (L\theta/2\pi) + (\delta/2)$. Making use of (17), we get the dispersion relation

$$D(\omega, k, l, \phi) = \sum_n \frac{\sin(k_n\delta/2)}{k_n\delta/2}\Gamma_n(\omega, k, l, \phi) = 0 \quad (24)$$

where the function Γ_n is defined by

$$\Gamma_n(\omega, k, l, \phi) = \left\{\eta_n^2\left(\tan\phi - \frac{k_n n}{\eta_n p_n}\right)^2\frac{J_n(\eta_n)}{J_n(\zeta_n)} \times\left[J_n(\zeta_n)N_n(\eta_n) - J_n(\eta_n)N_n(\zeta_n)\right] + \frac{\omega^2 R_h^2}{c^2}\frac{J_n'(\eta_n)}{J_n'(\zeta_n)}\left[J_n'(\zeta_n)N_n'(\eta_n) - J_n'(\zeta_n)N_n'(\zeta_n)\right]\right\} \quad (25)$$

$k_n = k - 2\pi(n-l)/L$, and ζ_n, η_n and p_n are defined in (11). The dispersion relation in (24), combined with (25), is one of the main results of this paper and can be used to investigate properties of the EM waves in a tape-helix waveguide for a broad range of system parameters.

Obviously the dispersion relation in (24) is a very complicated transcendental function of ω and k. However, in the limiting case when the outer conducting wall approaches to the helix (i.e., $R_c \to R_h$), the dispersion relation in (24) can be simplified to

$$\sum_n \frac{\sin(k_n\delta/2)}{k_n\delta/2}\left\{\zeta_n^2\left(\tan\phi - \frac{k_n R_h n}{\zeta_n^2}\right)^2 \frac{J_n(\eta_n)}{J_n(\zeta_n)} - \frac{\omega^2 R_h^2}{c^2}\frac{n^2-\zeta_n^2}{\zeta_n^2}\frac{J_n'(\eta_n)}{J_n'(\zeta_n)}\right\} = 0. \quad (26)$$

The helix mode [18] is obtained by further simplifying (26) to

$$\sum_n \frac{\sin(k_n\delta/2)}{k_n\delta/2}\left\{\omega^2 - \left[k_n c\sin\phi + n(c/R_c)\cos\phi\right]^2\right\} \quad (27)$$

where use has been made of the approximation $J_n(\eta_n)/J_n(\zeta_n) = 1$ and $J_n'(\eta_n)/J_n'(\zeta_n) = 1$. Making use of (1), it is straightforward to show that (27) is further reduced to

$$\left\{\omega^2 - \left[kc\sin\phi + l(c/R_c)\cos\phi\right]^2\right\}\sum_n \frac{\sin(k_n\delta/2)}{k_n\delta/2} = 0 \quad (28)$$

from which we obtain the helix mode

$$\omega = \pm\left[kc\sin\phi + l(c/R_c)\cos\phi\right] \quad (29)$$

for $R_c \to R_h$. It is remarkable to note from (29) that the helix mode is a straight line in the (ω, k) parameter space. Equation (29) is identical to the result obtained by authors [18] for a sheath helix waveguide. Moreover, this mode is independent of the width δ of the helix tape for $R_c \to R_h$. Obviously from (29), we also conclude that there is *no* forbidden region in the (ω, k) parameter space for the helix mode in a tape-helix-loaded waveguide, which is contrary to properties of the helix mode in a tape helix without outer conducting wall [3], [4]. The linear dependence of the eigenfrequency ω on the axial wavenumber k is particularly important in connection with application on the wide-band microwave amplifications.

In order to further investigate properties of the dispersion relation in (26), we first analyze the function defined by

$$f(x) = J_n(Rx)/J_n(x) \quad (30)$$

where R is a real quantity satisfying $0 < R < 1$. Apparently the function $f(x)$ has singularity at $x = \beta_{ns}$ where β_{ns} is the sth root of $J_n(\beta_{ns}) = 0$. Shown in Fig. 2 are plots of f versus x for $n = 3$, $s = 1$ and several values of R. Obviously from Fig. 2, we note that the function f changes very rapidly at $x \simeq \beta_{31} = 6.38016$. From (30), it can be shown

$$f(\beta_{ns} + \Delta) - f(\beta_{ns} - \Delta) = -\beta_{ns}(1-R)/\Delta \quad (31)$$

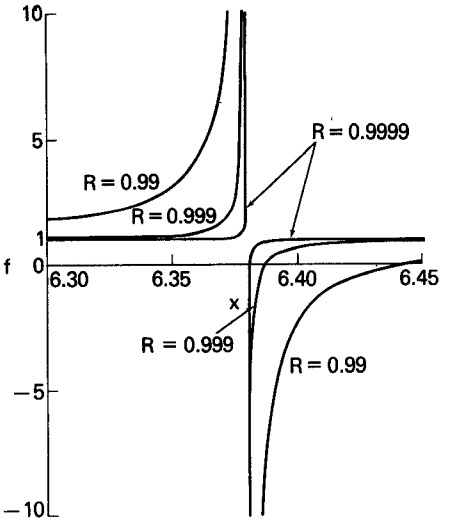

Fig. 2. Plots of the function $f(x) = J_n(Rx)/J_n(x)$ versus x for $n = 3$, $s = 1$ and several values of R.

for $R \to 1$ and $\Delta \ll 1$. We, therefore, conclude from (31) and Fig. 2 that for $R \to 1$, the function f will be any value between the negative and positive infinities by slightly changing the argument x from $x = \beta_{ns}$. In this context, there is always a value of ζ_n very close to β_{ns}, which satisfies (26) for $R_c \to R_h$. This mode is identified by the transverse magnetic-like (TM-like) mode

$$\frac{\omega^2}{c^2} - k_n^2 = \frac{\zeta_n^2}{R_c^2} = \frac{\beta_{ns}^2}{R_c^2}. \quad (32)$$

In a similar manner, from (26), we also identify the transverse electric-like (TE-like) mode

$$\frac{\omega^2}{c^2} - k_n^2 = \frac{\alpha_{ns}^2}{R_c^2} \quad (33)$$

in the limit $R_c \to R_h$. In (33), α_{ns} is the sth root of $J_n'(\alpha_{ns}) = 0$. Replacing k_n in (32) and (33) by k gives familiar TM and TE dispersion relations in an ordinary waveguide.

Finally, we point out that in the limit of $R_c \to \infty$, the dispersion relation in (24) can be simplified to

$$\sum_n \left\{q_n^2\left(\tan\phi + \frac{k_n R_h n}{q_n^2}\right)^2 I_n(q_n)K_n(q_n) + \frac{\omega^2 R_h^2}{c^2} I_n'(q_n)K_n'(q_n)\right\}\frac{\sin(k_n\delta/2)}{k_n\delta/2} = 0 \quad (34)$$

where $q_n^2 = -\eta_n^2$, and $I_n(x)$ and $K_n(x)$ are the modified Bessel functions of the first and second kinds, respectively, of order n. Equation (34) is identical to the result obtained by Sensiper [4].

III. Properties of Dispersion Relation

After a careful examination of (24) and (25), we obtain the following symmetry relation

$$D(\omega, k, l, \phi) = D(\omega, k + 2\pi l/L, 0, \phi) = D(-\omega, k, l, \phi) = D(\omega, -k, -l, \phi) \quad (35)$$

from which one notes two important properties. First, dispersion curves of the EM waves are symmetric about $\omega = 0$ line. Second, dispersion curves for space harmonic number l are generated from those for $l = 0$, by simply replacing k by $k + 2\pi l/L$ in the (ω, k) parameter space. In this regard, without loss of generality, analysis of (24) in this section is restricted to the positive eigenfrequency $(\omega > 0)$ and $l = 0$ mode.

The dispersion relation in (24) and (25) is numerically investigated for a broad range of system parameters R_c/R_h, ϕ, δ/L, and l. Even a numerical calculation of (24) is very complicated. After a careful examination of (24) and (25), we observe the following. Because the function $\sin x/x$ has the maximum amplitude at $x = 0$, the dispersion relation in (24) is dominated by the component n corresponding to a smallest absolute value of k_n. In this regard, we note from (6) that the value of n corresponding to the dominant component in (24) increases as the axial wavenumber k increases. For a moderately large value of δ/L $(0.2 < \delta/L < 0.5)$ and the $l = 0$ space harmonic mode, the dispersion curves near

$$k = (n/R_h)\cot\phi \tag{36}$$

can be approximately represented by

$$\Gamma_n(\omega, k, 0, \phi) = 0 \tag{37}$$

which incidentally has an identical form to the dispersion relation of a sheath helix [18] for the azimuthal harmonic number n. From the previous analysis [18] of the sheath helix dispersion properties, it has been shown that for specified value of ϕ and n, the minimum value of ω at $k = (n/R_h)\cot\phi$ satisfies

$$\omega \geq n(c/R_c)\cos\phi \tag{38}$$

for any values of R_c/R_h. Combining (36) and (38), we, therefore, conclude that for the $l = 0$ space harmonic mode, all dispersion curves in the region defined by $\omega \geq 0$ and $k \geq 0$ must satisfy

$$\omega \geq kc(R_h/R_c)\sin\phi. \tag{39}$$

Dependence of dispersion properties on the parameter R_c/R_h is illustrated in Fig. 3 where the normalized eigenfrequency $\omega R_h/c\cos\phi$ (solid curves) are plotted versus the normalized axial wavenumber $kR_h\tan\phi$ for $l = 0$ helix mode, $\phi = \pi/6$, $\delta/L = 0.3$, and (a) $R_c/R_h = 1.1$; (b) $R_c/R_h = 1.5$; (c) $R_c/R_h = 2$; and (d) $R_c/R_h = 5$. Two dashed straight lines represent $\omega = kc\sin\phi$ and $\omega = kc(R_h/R_c)\sin\phi$ from (29) and (39), respectively. Several points are noteworthy from Fig. 3. First, dispersion curves of the helix mode approach to the straight line defined by (29) as the parameter R_c/R_h is reduced to unity. Second, the dispersion curves of the helix mode wiggle more prominently as the parameter R_c/R_h increases from unity to infinity. Third, the helix dispersion curves overall approach to the line $\omega = kc(R_h/R_c)\sin\phi$ as the parameter R_c/R_h

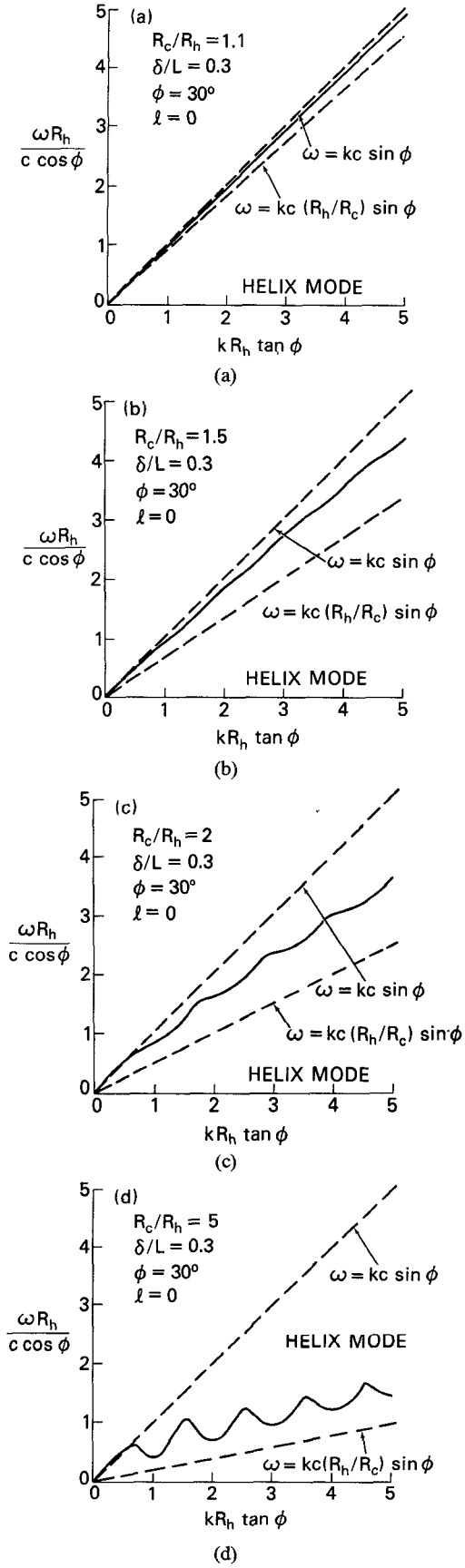

Fig. 3. Plots of normalized eigenfrequency $\omega R_h/c\cos\phi$ (solid curves) versus normalized axial wavenumber $kR_h\tan\phi$ obtained from (24) and (25) for $l = 0$ helix mode, $\phi = \pi/6$, $\delta/L = 0.3$. (a) $R_c/R_h = 1.1$. (b) $R_c/R_h = 1.5$. (c) $R_c/R_h = 2$. (d) $R_c/R_h = 5$.

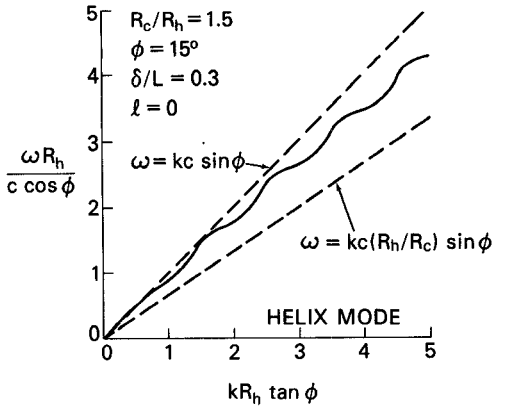

Fig. 4. Plot of normalized eigenfrequency $\omega R_h/c\cos\phi$ versus $kR_h\tan\phi$ obtained from (24) and (25) for $\phi = \pi/12$, $R_c/R_h = 1.5$ and parameters otherwise identical to Fig. 3.

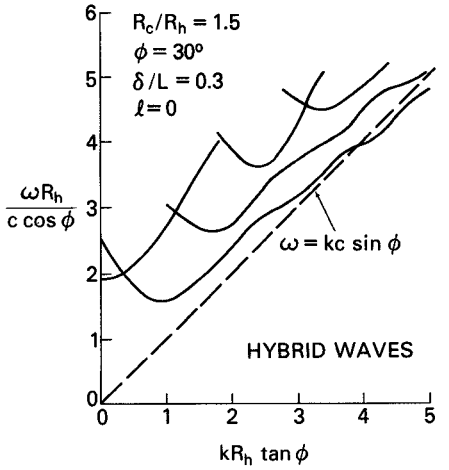

Fig. 5. Plots of normalized eigenfrequency $\omega R_h/c\cos\phi$ versus $kR_h\tan\phi$ obtained from (24) and (25) for $R_c/R_h = 1.5$, $l = 0$ hybrid waves and parameters otherwise identical to Fig. 3.

increases to infinity. Obviously, in the limit $R_c/R_h \to \infty$, every minimum points of ω in the dispersion curves are equal to zero where the line $\omega = kc(R_h/R_c)\sin\phi$ is merely simplified to $\omega = 0$. Shown in Fig. 4 is a plot of the normalized eigenfrequency $\omega R_h/c\cos\phi$ versus $kR_h\tan\phi$ obtained from (24) and (25) for $\phi = \pi/12$, $R_c/R_h = 1.5$ and parameters otherwise identical to Fig. 3. From a comparison of Fig. 4 with Fig. 3(b), we observe that the helix-mode dispersion curve wiggles more notably as the pitch angle ϕ reduces to zero.

We conclude this section by presenting plots of the normalized eigenfrequency $\omega R_h/c\cos\phi$ in Fig. 5 versus $kR_h\tan\phi$ obtained from (24) and (25) for $R_c/R_h = 1.5$, $l = 0$ hybrid waves and parameters otherwise identical to Fig. 3. Here the *hybrid* waves are defined by all the possible eigenmodes in the dispersion relation in (24), except the helix mode. There are infinite numbers of hybrid waves. Few examples of these waves are shown in Fig. 5. From the numerical analysis, we note that for $R_c/R_h \neq 1$, all the dispersion curves of the hybrid waves approach to the line $\omega = kc\sin\phi$ as the axial wavenumber k increases to infinity.

IV. Conclusions

In this paper, we have investigated properties of the EM wave propagation in a tape-helix-loaded waveguide. In deriving the dispersion relation of the wave, we assumed that the current in the tape flows only in the tape direction and that it does not vary in phase or amplitude over the width of the tape. In the limit $R_c/R_h \to 1$, it has been shown that the helix mode in a tape helix is identical to that of a sheath helix, thereby not depending on the width of helix tape. Moreover, presence of the outer conducting wall completely eliminates the forbidden regions usually appearing in a tape-helix theory. From numerical analysis of the dispersion relation, we found that the dispersion curves of the helix mode wiggle more prominantly as the outer conducting wall is further removed from the helix to infinity. In addition, it has been also found that there are infinite numbers of hybrid waves which mostly consist of a combination of the TE- and TM-like modes.

Finally, a preliminary study on the gyrotron amplifier in a tape-helix-loaded waveguide has been carried out. This study exhibits a strong coupling between the electron cyclotron mode and the hybrid waves, indicating possibilities of the microwave amplifications by a hybrid fast wave. However, theoretical analysis of the gyrotron amplifier in a tape-helix waveguide is very complicated and is currently under intensive investigation by authors. The results of this work will be published elsewhere.

Acknowledgment

We appreciate Dr. S. Ahn for providing us some of the references related to this topic.

References

[1] J. R. Pierce, *Travelling-Wave Tubes*. New York: Van Nostrand, 1950, ch. 3.
[2] R. G. E. Hutter, *Beam and Wave Electrons in Microwave Tubes*. New York: Van Nostrand, 1960, ch. 7.
[3] D. A. Watkins, *Topics in Electromagnetic Theory*. New York: Wiley, 1958, ch. 2.
[4] S. Sensiper, *Proc. IRE*, vol. 43, p. 149, 1955.
[5] C. Shulman and M. S. Heagy, *R.C.A. Reviews*, vol. 8, p. 585, 1947.
[6] D. A. Watkins and A. E. Siegman, *J. Appl. Phys.*, vol. 24, p. 917, 1953.
[7] C. O. Lund, *R.C.A. Review*, vol. 11, p. 133, 1950.
[8] W. Sichak, *Proc. IRE*, vol. 42, p. 1315, 1954; also J. H. Bryant, *Elec. Commun.*, vol. 31, p. 50, 1954.
[9] A. K. Berezin, P. M. Zeidlits, A. M. Nekrshevich, and G. A. Silenok, *Soviet Phys. Tech. Phys.*, vol. 4, p. 730, 1960.
[10] S. P. Morgan and J. A. Young, *Bell System Tech.* J, vol. 35, p. 1347, 1956.
[11] V. A. Flyagin, A. V. Gaponov, M. I. Petelin, and V. K. Yulpatov, *IEEE Trans. Microwave Theory Tech.*, vol. MTT-25, p. 514, 1977.
[12] J. L. Hirschfield and V. L. Granatstein, *IEEE Trans. Microwave Theory Tech.*, vol. MTT-25, p. 528, 1977.
[13] H. S. Uhm and R. C. Davidson, *Phys. Fluids*, vol. 23, p. 2538, 1980.
[14] J. Y. Choe, H. S. Uhm, and S. Ahn, *J. Appl. Phys.*, vol. 52, p. 7067, 1981.
[15] A. Palevsky and G. Bekefi, *Phys. Fluids*, vol. 22, p. 986, 1979.
[16] D. A. G. Deacon, L. R. Elias, J. M. M. Madey, G. J. Ramian, H. A. Schwettman, and T. I. Smith, *Phys. Rev. Lett.*, vol. 38, p. 897, 1977.
[17] H. S. Uhm and R. C. Davidson, *Phys. Fluids*, vol. 24, p. 1541, 1981.
[18] H. S. Uhm and J. Y. Choe, "Properties of the electromagnetic wave propagation in a helix loaded waveguide," *J. Appl. Phys.*, vol. 53, p. 8483, 1982.

Han S. Uhm received the B.S. degree from Seoul National University, Seoul, Korea, in 1969, the M.S. degree from the University of Maryland, College Park, in 1973, and the Ph.D. degree also from the University of Maryland in 1976, all in physics.

Since joining the Naval Surface Weapons Center in 1978 in the Nuclear Branch, he has worked as a Plasma Research Physicist. His research has included work on charge beam propagation in a background plasma, collective ion acceleration, beam properties in a particle accelerator, high-power microwave generation, non-neutral plasma, thermonuclear magnetic confinement, and electron and positron beams in a storage ring.

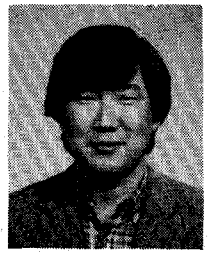

Joon Y. Choe was born in Seoul, Korea, and received the B.S. and Ph.D. degrees in physics from the Seoul National University and the University of Kansas, Lawrence, respectively.

He worked on fusion plasma stability at the Courant Institute and the University of Maryland, College Park, and on microwave generation at the Naval Research Laboratory. Since joining the Naval Surface Weapons Center, he has been engaged in research on microwave generation, waveguide theory and experiment, particle accelerator theory, and computer simulations.

Mode-Specific Reflectometry in a Multimode Waveguide

DAVID S. STONE, MEMBER, IEEE, KEVIN L. FELCH, AND STEPHEN T. SPANG, MEMBER, IEEE

Abstract—**A technique for measuring the voltage-standing-wave ratio (VSWR) created by a mismatch for a specific mode in a multimode waveguide is described. A heavily loaded resonant cavity is used to launch the mode of interest and the variation in the cavity loaded Q is noted as the phase separation of the cavity and the mismatch is varied. The bandwidth of this technique is generally about 0.03 percent and VSWR as low as 1.05:1 may be measured accurately. Mode-specific VSWR measurements are of particular interest in analyzing the performance of multimode waveguide components, and in optimizing multimode networks. The measurement technique may be used, for example, in the design and optimization of transmission lines for electron cyclotron resonance heating systems in magnetic fusion devices.**

I. Introduction

RECENT ADVANCES in high average power millimeter-wave devices, such as the gyrotron [1], [2], have aroused interest in the use of multimode waveguides for handling power levels which would produce excessive power densities in single-mode systems. Millimeter-wave sources of this type are susceptible to mode competition [3], which is aggravated by reflections of either the principal mode of interest or of the competing modes. It is, therefore, particularly important to be able to characterize a multimode waveguide system by measuring the voltage-standing-wave ratio (VSWR) for several specific modes of interest in the system.

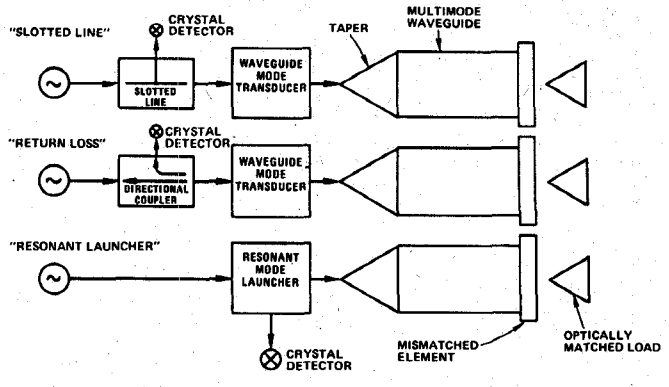

Fig. 1. Schematic diagram of three VSWR measurement techniques in multimode waveguide.

Conventional reflection measurements in waveguides are made using commercially available transducers to launch the waveguide mode of interest (see Fig. 1). Standard millimeter-wave test equipment is designed for the $TE_{10}^{\square}$ (fundamental rectangular) mode, whereas overmoded transmission lines, as employed in long-distance telephone links [4], or gyrotron collector structures [5], are typically cylindrical. Thus transducers designed to produce mode transformations of the type $TE_{10}^{\square} \leftrightarrow TE_{mn}^{\circ}$ and $TE_{10}^{\square} \leftrightarrow TM_{mn}^{\circ}$ are required. Only the simplest of these waveguide components, the $TE_{10}^{\square} \leftrightarrow TE_{11}^{\circ}$ transducer is available with

Manuscript received September 15, 1982; revised April 15, 1983. This work was supported by a grant from the Oak Ridge National Laboratory, which is operated by the Union Carbide Corporation for the U.S. Department of Energy under Contract W-7405-eng-26.

The authors are with Varian Associates, Inc., 611 Hansen Way, Palo Alto, CA 94303.

0018-9480/83/0900-0710$01.00 ©1983 IEEE